A Composite Rigid Double Cantilever Beam Specimen for Assessing the Traction-Separation Response of Mode I Delamination in Composite Laminates

Devon C. Hartlen, John Montesano, Duane S. Cronin*

Department of Mechanical and Mechatronic Engineering, University of Waterloo, 200 University Ave W, Waterloo, ON, CA, N2L 3G1

*Corresponding author. Email: duane.cronin@uwaterloo.ca

Contributing authors: devon.hartlen@uwaterloo.ca; john.montesano@uwaterloo.ca

Abstract

Background

Interlaminar delamination is a common damage mechanism in composite laminates that can lead to structural failure. Assessment using contemporary numerical modeling techniques requires delamination behavior as a traction-separation response. However, existing experimental characterization approaches are not well suited to support these modeling techniques as specimens were developed to assess single delamination parameters, not a full traction-separation response, or utilize analysis schemes that require knowledge of material properties.

Objective

To develop a test specimen and data analysis methodology to directly measure the traction-separation response of Mode I delamination in a laminated fiber-reinforced polymer (FRP) composite, including strength, toughness, and damage response.

Methods

The proposed composite Rigid Double Cantilever Beam (cRDCB) specimen is comprised of a [0]_4 unidirectional E-glass/epoxy laminate co-cured to rigid metallic adherends. Traction-separation response was assessed directly from measured force and displacement behavior using a closed-form analysis scheme that does not require a priori knowledge of composite material properties. Standard double cantilever beam (DCB) tests were performed for comparison.

Results

The cRDCB specimen captured early damage initiation and progression in greater detail than the DCB, with measured strain energy release rates agreeing well between the two approaches. The cRDCB also captured the effects of large-scale damage mechanisms such as fiber bridging. The measured traction-separation responses are suitable for scenarios where prediction of the initiation and early damage response of delamination is important.

Conclusions

Combined with a data processing technique, a single cRDCB test enabled measurement of the full Mode I traction-separation response. In addition, the cRDCB provided high-resolution and could detect early-stage Mode I delamination damage in FRP laminates. The measured traction-separation responses can be directly inputted into cohesive zone models to predict the initiation and progression of Mode I delamination.

Keywords: Delamination, Characterization, Composite Laminates, Traction-Separation Response, Rigid Double Cantilever Beam

1 Introduction

Interlaminar delamination is a widely observed damage mechanism for fiber-reinforced plastic (FRP) laminates and an important failure mode to consider when designing for damage-tolerant and energy-absorbing applications such

as transportation structures. Prediction of delamination initiation and growth is often accomplished using numerical modeling and techniques such as cohesive zone modeling (CZM). CZM is an effective and efficient technique for predicting delamination response [1]. However, it requires a detailed description of material behavior in the form of traction-separation responses (TSRs), which describe the complete evolution of delamination from damage onset to crack propagation (Fig. 1). Unfortunately, many existing experimental methods for assessing delamination in laminated composites are ill-suited to measuring TSRs as they were not originally developed for that task, which has led to the development of supplemental analysis schemes requiring a priori knowledge of material properties to calculate a TSR.

Driven by interlaminar stresses and constraint effects from adjacent plies, delamination behavior varies depending on loading direction and is often classified using the three archetypal fracture modes. Mode I delamination response, the focus of this research, can be broadly divided into two separate but related regimes. First is a fracture process zone (FPZ) that exists ahead of the crack tip (Fig. 1, Region 2). The response of the FPZ is driven largely by matrix behavior, and owing to the constraint stemming from fibers in the adjacent lamina, the size of the FPZ is relatively small [2, 3]. As damage accumulates and overwhelms the matrix material, the crack tip and FPZ advance into previously undamaged material. In their wake, the second regime of large-scale fiber bridging (Fig. 1, Region 3) begins to dominate. Fibre bridging acts as a crack shielding mechanism that further increases resistance to crack extension [4]. Both damage regimes are affected by a range of factors, such as fibre-matrix interface properties [1, 5–7], processing methodology [7], and specimen dimensions [2, 3, 8].

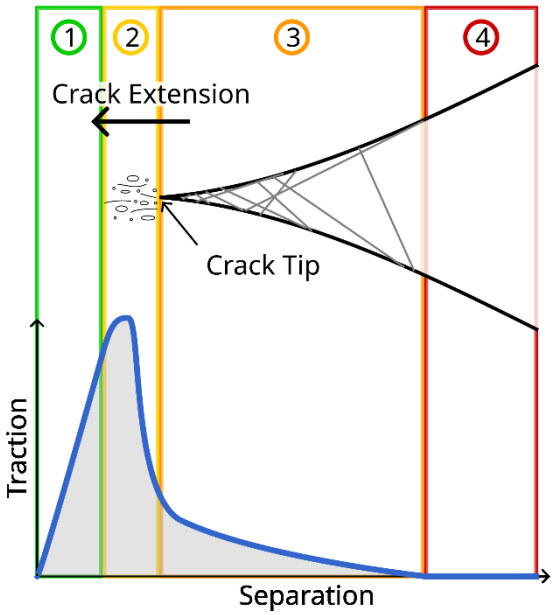

Fig. 1 A schematic of damage evolution for Mode I delamination and representative traction-separation response (TSR). Region 1) undamaged material that exhibits a linear elastic response. Region 2) A matrix-dominated fracture process zone (FPZ) ahead of the crack tip. Region 3) An extended region dominated by large-scale fiber bridging produced by the crack extending through this region, characterized by low tractions for extended separations. Region 4) Fully damaged material providing no damage resistance and, hence, no traction. The shaded region under the TSR is equivalent to the strain energy release rate (SERR).

The widely used and accepted technique for characterizing Mode I delamination in composite laminates is the double cantilever beam (DCB) specimen (Fig. 2a) [6]. The DCB was developed to assess the delamination toughness of a laminate in the form of strain energy release rate (SERR). While toughness is a key damage parameter (the area under the TSR, Fig. 1), it is insufficient to characterize a TSR fully, requiring additional tests or inverse modeling. However, additional tests with alternate geometries are time-consuming and expensive, while the DCB specimen is not well suited to inverse modeling due to a lack of sensitivity in assessing damage onset and early accumulation behavior [9, 10].

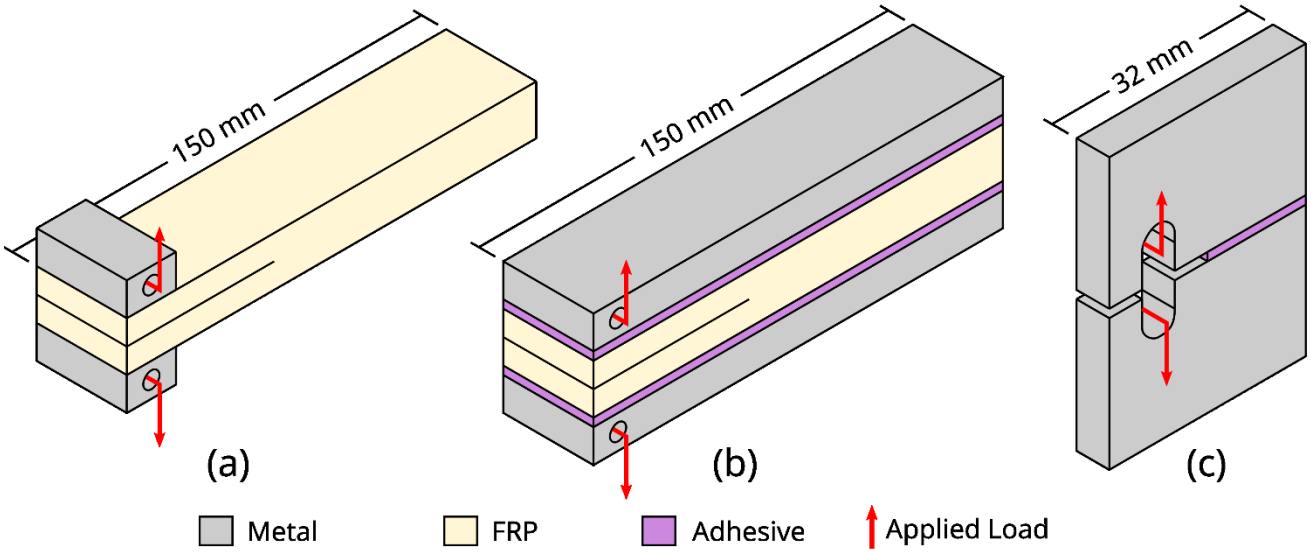

Fig. 2 Schematic of the DCB specimen (a) and two alternative specimens, the reinforced double cantilever beam (b) and the RDCB (c). Specimens are not to scale, but a typical major dimension for each is provided.

Data processing schemes have been introduced to extract the TSR from DCB specimens, mainly based on applying the J-integral [11–14]. These techniques have had success in capturing the later stages of damage but require the stiffness of the laminate to be known a priori, require the specimen to be loaded with a pure moment [12], or measurement of the rotation of the DCB arms [13, 15], and have difficulty assessing the early portions of a TSR corresponding to damage onset and accumulation [16]. To that end, alternative specimens have been put forth to assess the TSR of interlaminar delamination better.

Marzi et al. [17] developed the reinforced DCB specimen (Fig. 2b), consisting of aluminum blocks adhered to either side of a standard DCB specimen. The known, comparably high stiffness of the aluminum blocks enabled researchers to apply the J-integral technique to extract a TSR without knowledge of laminate stiffness. However, while the reinforced DCB simplified the measurement of TSR, the specimen shares the same lack of resolution of early damage behavior as the traditional DCB specimen.

Another alternative, developed by Dastjerdi et al. [18] and enhanced by Watson et al. [19] for characterizing the TSR of structural adhesives, is the rigid double cantilever beam (RDCB, Fig. 2c). The RDCB consists of relatively small metallic adherends (approximately one-fifth the overall length of a DCB specimen) bonded together with the adhesive of interest. While this specimen exhibits some visual similarities to the compact tension (CT) specimen

for metals [20], the RDCB specimen uses a unique data processing technique to extract the complete TSR of the adhesive from force and specimen displacement. Additionally, the small size of the specimen makes it suitable for high-deformation rate testing, a requirement for adoption in the transportation industry. The RDCB specimen has been successfully used for ductile structural adhesive [19] and uncured thermosets tows [21] but has not been investigated for strong, stiff materials with complex damage mechanisms, such as laminate FRPs.

The current study developed a new specimen and analysis methodology to characterize the Mode I delamination behavior of FRP laminates. The new specimen, designated the composite rigid double cantilever beam (cRDCB), consists of effectively rigid metallic adherend co-cured to an FRP laminate. Adapting the data processing methodology of Watson et al. [19] for use with much stiffer composite laminates, the cRDCB can extract the entire TSR of a delamination interface from a single test geometry. Further, the compact nature of the cRDCB, in concert with digital image correlation (DIC) analysis, enables detailed assessment of damage onset and progression. Finally, the performance of the cRDCB specimen is compared to the DCB specimen based on SERR.

2 Methodology

2.1 Composite Rigid Double Cantilever Beam (cRDCB) Specimens

cRDCB specimens were produced through a co-curing process to replicate compression molding (Fig. 3). Mild steel adherends were prepared for co-curing by roughening the surface interfacing with the GFRP to a minimum surface roughness of 2.0 μm r_a using abrasive blasting media to help ensure a good connection between GFRP and adherends. Individual unidirectional laminates comprising four plies ($[0]_4$) were prepared for each cRDCB specimen from unidirectional E-glass prepreg tape (UE400/REM, CIT, Italy), with a 12.5 μm PTFE film placed at the midplane of the laminate to serve as a crack initiator. The completed laminate was sandwiched between the two steel adhered with the fiber direction parallel to the long edge of the adherend and placed in a custom-developed curing fixture. This curing fixture provided a consistent pressure of 0.5 MPa during curing, confinement of the GFRP material, and controlled the thickness (1.05 mm (SD=0.05 mm)) and volume fraction of the GFRP. Curing took place in an oven at 140°C for 90 minutes. Once cured, excess resin and spew were removed from the specimens

using abrasive paper. The average fiber volume fraction of cRDCB specimens was 47%, with a density of 1.72 g/cm^3 as measured with acid digestion [22].

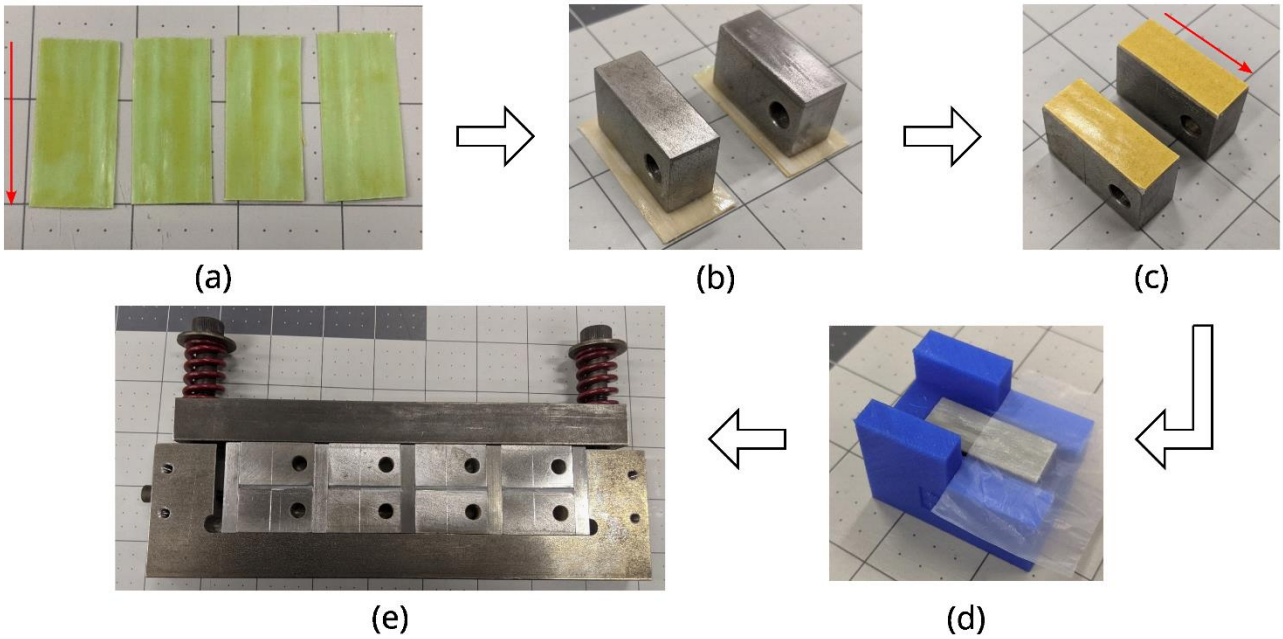

Fig. 3 A summary of the cRDCB manufacturing process. (a) Pre-preg tapes are cut oversized, then stacked into sub-laminates, and (b) pressed to the roughened metallic adherends. (c) Sub-laminates were trimmed to size then (d) a PTFE film crack starter was placed with the aid of a jig to ensure good repeatability. (e) Specimens were placed in a curing fixture that provided confinement and constant pressure during the cure cycle. Not shown in (e) is an additional plate clamped across the front of the specimens to provide confinement. The red arrows in (a) and (c) denote the fiber direction

Eight cRDCB specimens (Fig. 4) were tested in tension using a servo-electric universal test frame (AGX-50kN, Shimadzu, Japan) at a constant crosshead speed of 10^{-3} mm/s. Deformation of the GFRP was assessed using digital image correlation (DIC) measurements (VIC-2D, Correlated Solutions, USA). DIC enabled on-specimen measurement of the specimen displacement required for extracting traction-separation response and enabled assessment of damage accumulation and propagation behavior. Displacement for extracting traction-separation response was evaluated across the crack tip using a virtual extensometer (denoted with stars in Fig. 4), with the position of the initial crack tip position marked with a scribed line. Crack tip position is not required to extract traction-separation response; however, the full-field strain measurements provided by DIC enable visual estimation of the extent of delamination crack growth in a specimen.

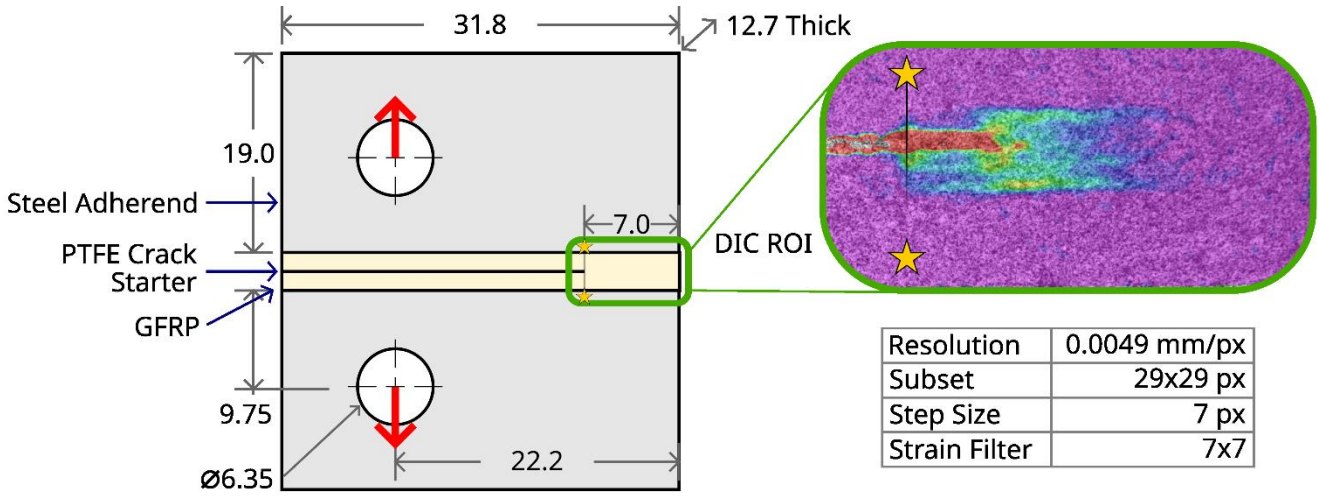

Fig. 4 Schematic of cRDCB specimen (left) with an inset showing DIC region of interest (right, first principal strain shown) and DIC processing parameters. Stars on the DIC region of interest demonstrate the points where specimen displacement was measured

The traction-separation response of the cRDCB specimen was extracted using the methodology laid out by Watson et al. [19] (reproduced in Appendix A). This methodology makes use of the first derivative of the force-displacement response. However, the direct calculation of the first derivative produced an extremely noisy response owing to experimental noise induced by the very small displacements measured with DIC (on the order of 10^{-2} mm or 2 pixels). To that end, a regression-type, a piecewise cubic spline [23] was fit to each force-displacement response. This approach not only allowed for the extraction of a continuous first derivative of force-displacement but also allowed physical constraints to be applied during the fitting process, such as enforcing linear behavior during the initial period of loading.

2.2 Double Cantilever Beam (DCB) Specimens

DCB specimens (Fig. 5a) were extracted from a processed laminate FRP panel consisting of 10 plies ($[0_{10}]$) of the same E-glass/epoxy as the cRDCB specimens with a 12.5 μm PTFE crack starter between plies 5 and 6. This layup was selected to target the lower end of specimen thickness specified by ASTM D5528 [3], assuming a thinner laminate would provide a more direct comparison to the cRDCB specimen. The panel was fabricated via compression molding in a hydraulic press with temperature-controlled platens (G100H-24, Wabash, USA) using the same temperature, pressure, and curing time as the cRDCB specimens. Waterjet cutting was used to extract

specimens from the GFRP panel. Load blocks, machined from mild steel per ASTM D5528 [6], were bonded to the specimens using a structural adhesive (Impact Resistant Structural Adhesive 7333, 3M Canada, London, Ontario). DCB specimens had a fiber volume fraction of 53% and density of 1.79 g/cm^3 as measured with acid digestion [22].

DCB specimens were loaded at a constant crosshead speed of 5 mm/min using the same test equipment used to test the cRDCB specimens. No crack conditioning was performed prior to testing. Open-sourced optical tracking software [24] was used to assess the opening of the DCB arms and monitor crack growth. A crack equivalence technique [25] was used to compute the resistance or R-curve and assess the delamination toughness of each specimen.

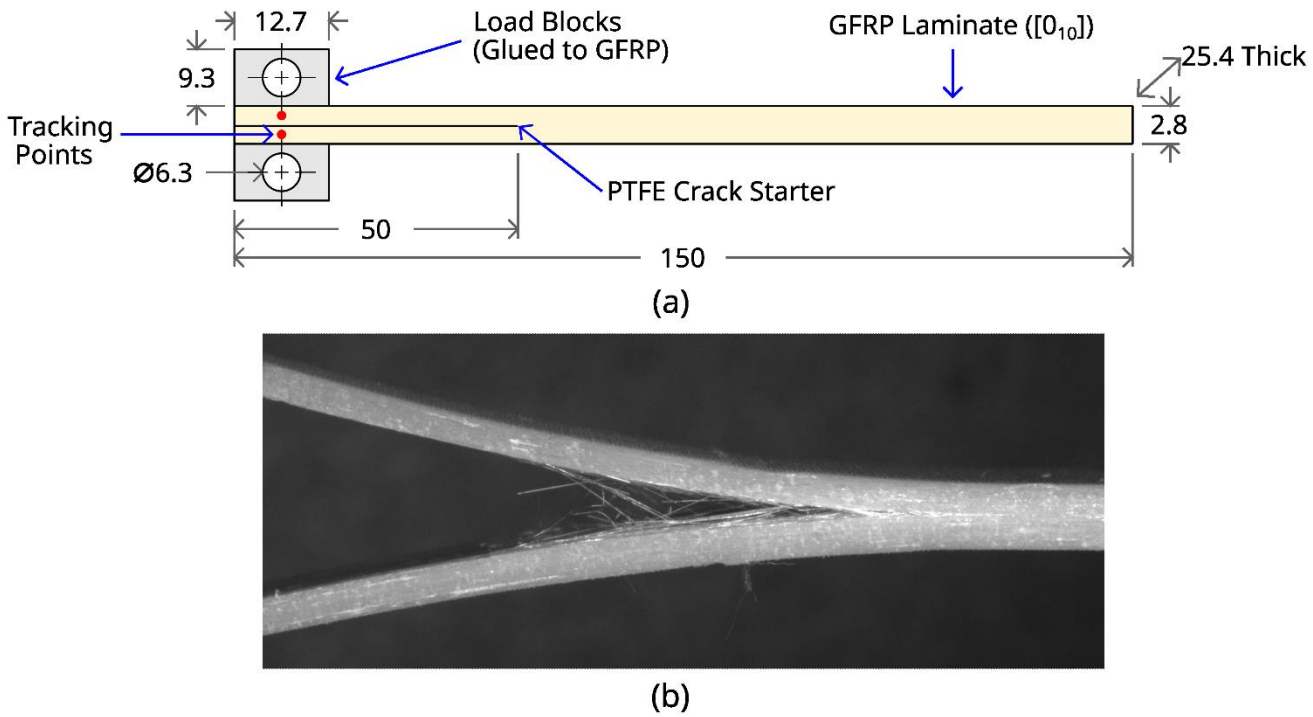

Fig. 5 (a) Dimensions of the DCB specimens used in this work (not to scale). (b) An image of a DCB specimen captured during testing exhibiting large-scale fiber bridging behind the crack tip.

3 Results and Discussion

3.1 cRDCB Experimental Results and Analysis

The specimens all broadly exhibited the same force-displacement response (Fig. 6): 1) a period of linear behavior of elastic deformation prior to damage initiation, 2) a period of mild non-linearity as damage initiated and began to

accumulate, 3) a “plateau” as the leading edge of the crack tip experienced significant matrix damage, and the crack tip began to advance, and 4) an unloading period as the crack tip advanced and large-scale fiber-bridging began to dominate the response. Of the eight cRDCB specimens tested, all but one experienced interlaminar delamination. The remaining specimen exhibited interfacial failure between the GFRP laminate and metallic adherend and was excluded from further analysis. Variability in the test results was attributed to two sources: placement of the PTFE tape, which could lead to small differences in interface length and affect the initial stiffness and strength of the specimen, and the condition of the crack tip, which could impact early damage behavior. Variability could also be amplified by the small size of the cRDCB specimen, as less material was being placed under load compared to traditional specimens, potentially exacerbating the effect of the quality of the composite laminate and features such as micro-voids and resin-rich zones. However, as will be noted later, the variability of the cRDCB specimen is on the same order of magnitude as the DCB specimens tested in this work.

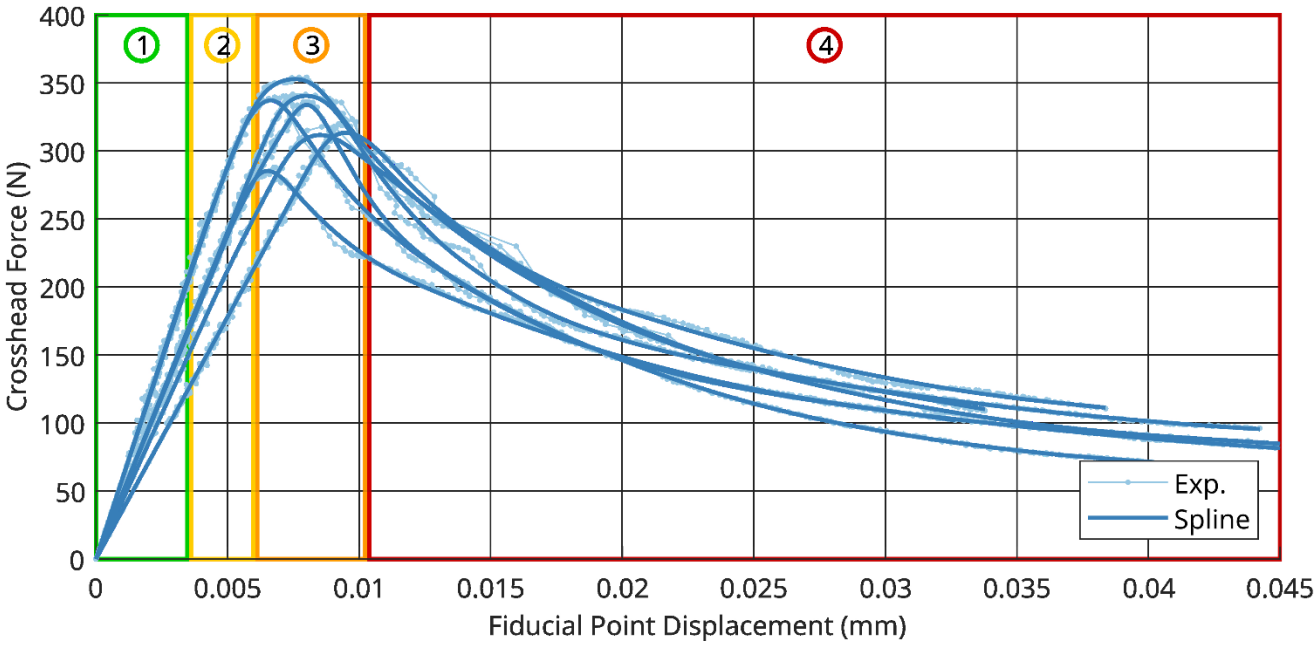

Fig. 6 Experimental force-displacement responses from cRDCB specimens (n=7) with overlaid smoothing splines. Four regions of material delamination response are highlighted, corresponding to Region 1) elastic behavior prior to damage initiation, Region 2) the start of non-linearity corresponding to damage imitation, Region 3) a “plateau” resulting from significant matrix damage and the start of crack propagation, and Region 4) unload period characterized by the domination of large-scale fiber bridging.

Examining full-field strain fields allowed damage progression to be correlated against the regions detailed above. During the period of elastic loading (Region 1, Fig. 7a), strain accumulated proportionally in the area ahead of the crack tip as well as the compressive region at the rear of the specimen. As loading continued, more damage accumulated at the crack tip (Regions 2 and 3, Fig. 7b). This process can be interpreted in the DIC strain fields as an increase in strain at the crack tip without the crack tip moving. It is important to note that measuring the exact location of the crack tip is not required to extract the traction-separation response from cRDCB specimens, nor is it an outcome of this work. However, full-field displacement measurement enables one to estimate the current crack tip position and growth by following the high strain concentration that naturally develops as crack tip displacement increases. During this period, compressive strains continue to increase linearly. Finally, as the crack advanced (Region 4, Fig. 7c), the strain contours allowed the extension of the crack to be tracked. The contours around the crack tip tend not to change shape during crack extension, although magnitudes may change dependent on the applied load. Compressive strains continued to respond linearly, indicating undamaged material behavior. DIC imagery also showed that the areas of highest tensile and compressive strain prior to crack propagation occurred at the interface between composite and adherend due to the large variation in stiffness between the two materials generating a constraining effect. This result emphasizes the importance of surface preparation to ensure a good bond between the composite and adherend during the co-curing process. Laminate thickness also influenced the intensity of these strains, which led to the use of a four-ply laminate used in this work.

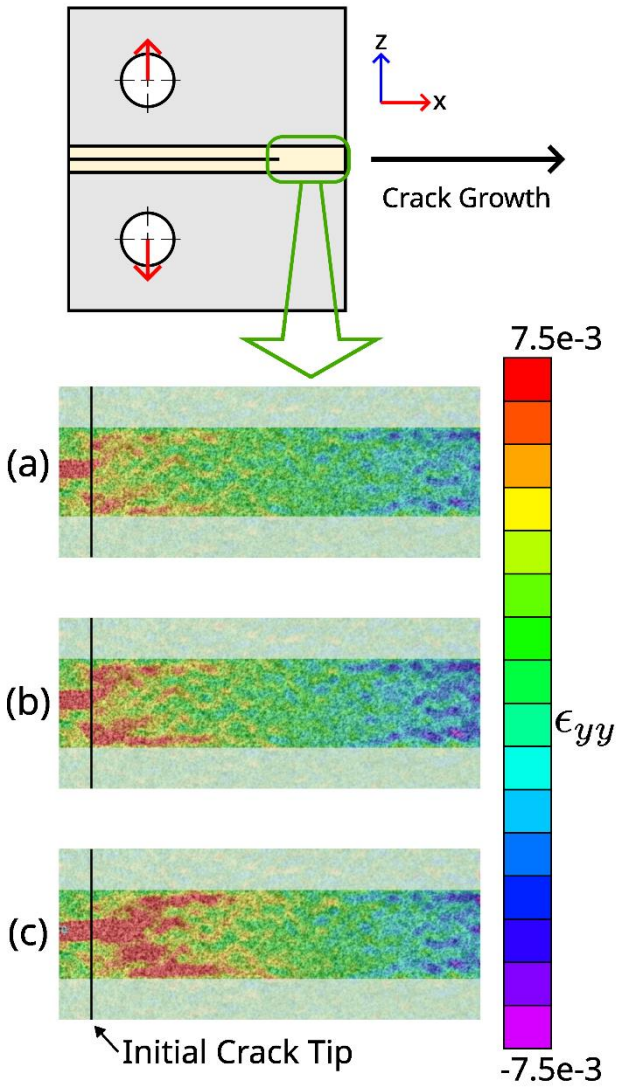

Fig. 7 Evolution of full-field strain during the crack propagation in the cRDCB specimen, from (a) elastic loading to (b) early evolution of the fracture process zone at the crack tip to (c) stable crack propagation with a fully established fracture process zone. The black line in each image indicates the initial location of the crack tip. The crack runs in the positive x-direction in these images

The extracted TSRs (Fig. 8), which captured the response of the delamination interface at the initial crack tip, exhibited some non-physical oscillation, mainly in the bridging response of the delamination interface. Extracting TSRs from cRDCB specimens required solving a differential equation influenced heavily by the first and second derivatives of force-displacement behavior. While smoothing splines helped significantly reduce oscillatory behavior, this phenomenon could not be fully eliminated. Additionally, it was found that the location of the inflection point in force-displacement behavior was directly tied to the transition from matrix-dominated behavior

to fiber-bridging-dominated behavior. If the smoothing splines did not accurately capture the location of this inflection point or if some unstable crack propagation occurred, significant oscillation could be introduced.

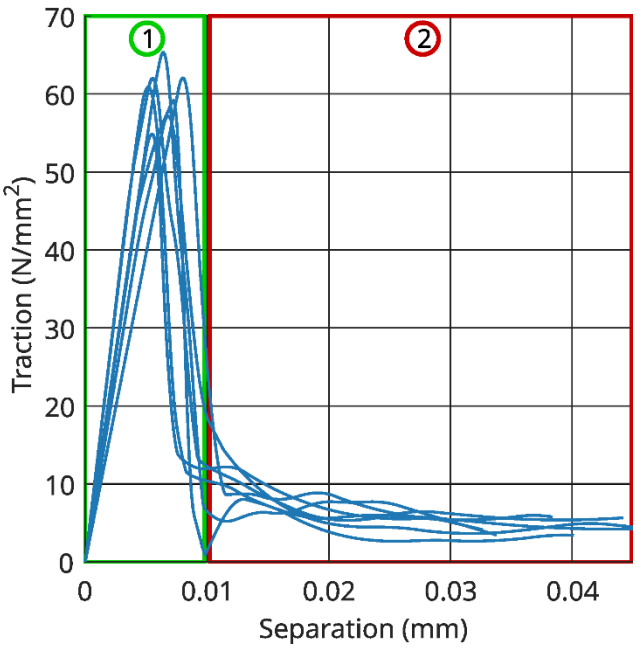

Fig. 8 Traction-separation responses (TSRs) extracted from splines fitted to experimental cRDCB data. Approximate extents of matrix-dominated behavior (1) and fiber-dominated behavior (2) are annotated.

SERR was computed by integrating the TSRs. However, TSRs extracted from the cRDCB specimens do not return to zero traction at large deformation, indicating the full extent of damage response was not evaluated due to the protracted bridging response of this material in concert with the length of the specimen. This result also indicated that a steady-state fibre bridging zone length was not established. While the length of the fibre bridging zone was difficult to measure given the small crack tip opening displacements, examination of DIC measurements, in concert with the size of the physical specimen, suggested the zone could not have been larger than 5-7 mm. SERR associated with matrix behavior (up to the inflection point in force-displacement response) was calculated to be 0.32 J/mm^2 (SD = 0.04 J/mm^2). To estimate the total SERR for Mode I delamination, a linear response was assumed to extrapolate each TSR out to zero traction. This approach produced an estimated SERR of 0.7 J/mm^2 at a final separation of approximately 0.15 mm. A linear response has been used to model large-scale fiber bridging in other works [2].

3.2 Experimental DCB Results and Analysis

The force-displacement responses of the DCB specimens ($n = 7$, Fig. 9a) demonstrated low variability. Force-displacement behavior could be described as roughly tri-linear, commencing with an initial linear response as the material was loaded through the elastic region, a second linear period of diminished slope as the crack began to advance and fiber-bridging began to form, and a final period of flat or slightly decreasing slope as the crack advanced with an established zone of large-scale fiber bridging. Crack propagation was stable, with only limited periods of stick-slip behavior.

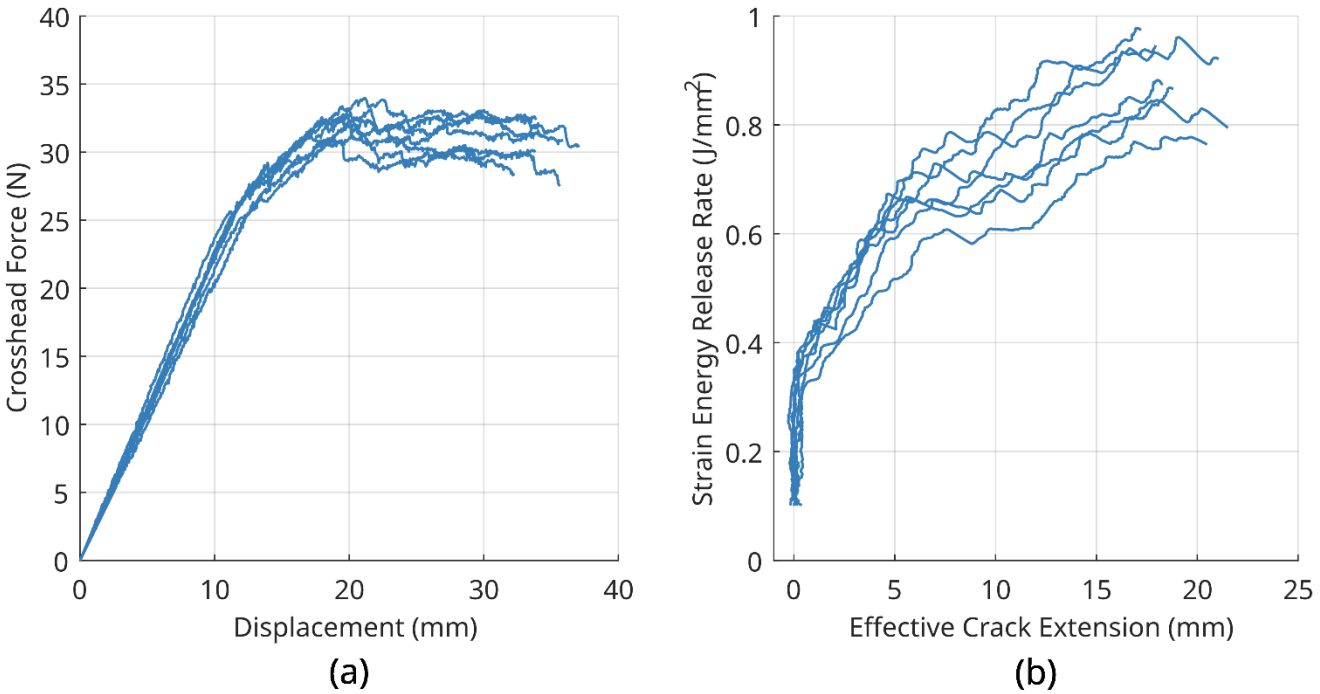

Fig. 9 Force-displacement (a) and R-curve (b) responses measured from experimental DCB testing (n=7 specimens). SERR and effective crack extension were evaluated with the crack-equivalence method [25]

R-curves for the DCB specimens (Fig. 9b) exhibited the classic rising trend associated with large-scale fiber bridging [2], although steady-state did not appear to be achieved with the crack extension reached during this work. Test imagery showed that the length of the fibre bridging zone did not appear to have reached a constant length during testing, further supporting the trend observed in extracted R-curves. However, the R-curves trend toward a steady-state somewhere between 0.8-1.1 J/mm^2, which is typical of this class of E-glass/epoxy laminate [26, 27].

R-Curves exhibit an average toughness at the onset of crack growth of 0.35 J/mm^2 (SD = 0.03), although the insensitivity of the DCB specimen to early damage behaviour does produce some uncertainty in this measurement.

3.3 Comparison and Discussion of cRDCB and DCB Specimens

Despite the differences in geometry boundary conditions, microscopy (VHS-5000, Keyence, Japan) revealed that both the cRDCB and DCB (Fig. 10) exhibited similar fracture morphologies consistent with stable Mode I delamination such as matte, scalloped fracture surfaces on the matrix material, fiber-matrix interfacial debonding, and fiber breakage [28, 29]. A small number of voids were observed on the fracture surface of both specimens in patterns that indicated a lack of consolidation of the prepreg tapes. The prepreg tape used in this work was extremely resin rich, which could have inhibited full consolidation and complete elimination of voids to a small degree. However, there was no evidence that delamination initiated at these voids rather than the crack starter. The cRDCB specimens tended to exhibit more visible matrix damage than DCB specimens, perhaps due to the slightly lower fiber-volume fraction of these specimens. However, the prevalence of matrix damage may also help demonstrate that the cRDCB specimen has greater sensitivity to early damage behaviors, which are largely driven by the matrix material.

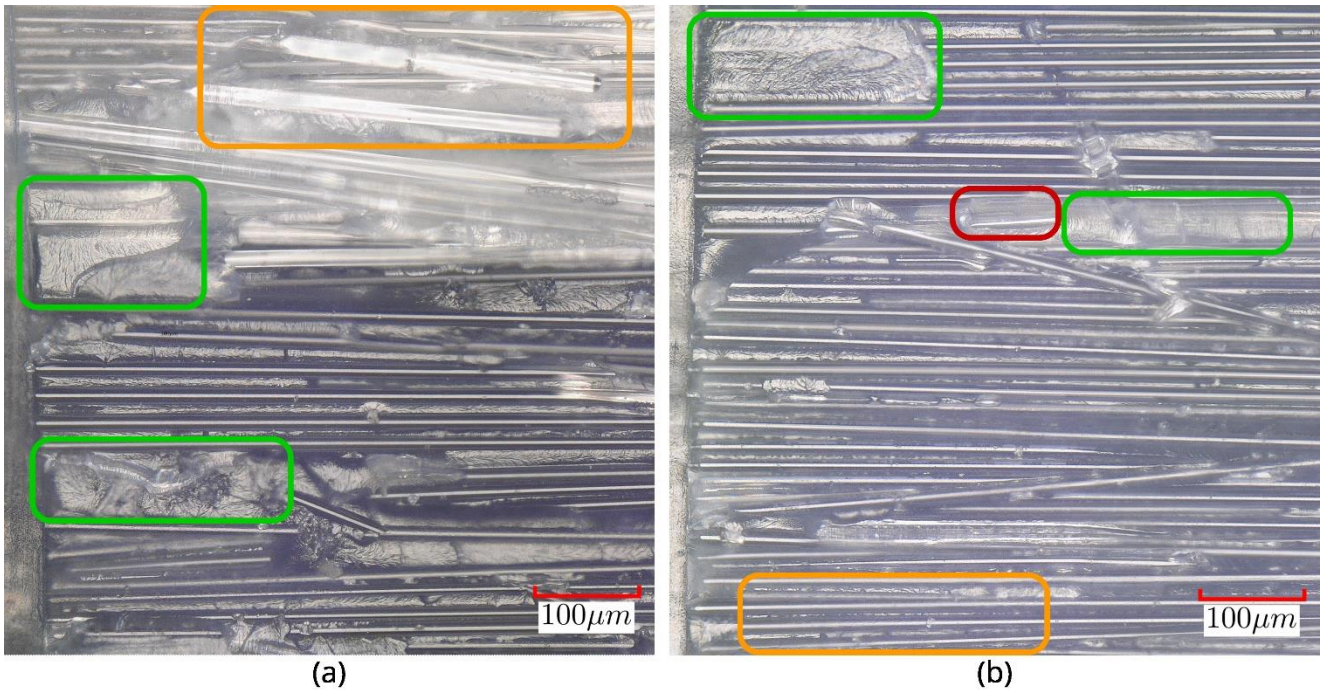

Fig. 10 Representative fracture surface imagery of the cRDCB (a) and DCB (b) specimens, with exemplar morphologies consistent with Mode I delamination highlighted: matte, scalloped surfaces on matrix material (green), fiber-matrix debonding (orange), and while not a delamination morphology, voids at the interface (red)

Overall, there was good agreement between the cRDCB and DCB specimens for early damage behavior with respect to SERR. Integrating the TSRs of the cRDCB up to the onset of bridging produced a SERR of 0.32 J/mm^2 (SD = 0.04), which agreed favorably with the initial toughness of the DCB specimens (where R-curves begin to deviate from vertical) of 0.35 J/mm^2 (SD = 0.03), both in terms of magnitude and variability. However, unlike the DCB specimen, the cRDCB provided much greater resolution when assessing the onset of delamination, as evidenced by the extracted TSRs (Fig. 8). The similarity in SERR between the cRDCB and DCB specimens in the early delamination regime also demonstrated that the matrix behavior was independent of the two specimen designs.

The cRDCB and DCB specimen responses diverged somewhat as fiber-bridging began to dominate the response of the specimens. The extrapolated total SERR of the cRDCB specimen was estimated to be 0.7 J/mm^2, while all DCB specimens exhibited a rising R-curve that trended greater than 0.8 J/mm^2. However, it is important to note that high SERR values in the DCB specimens only occurred at crack extensions of at least 20 mm, which was significantly greater than what is attainable for the cRDCB specimen. A more reasonable comparison would be to compare the

toughness of the DCB specimen at approximately 5 mm of crack extension, which is more reflective of the crack lengths possible using the cRDCB specimen. At 5 mm of crack extension, the DCB specimens had a SERR of 0.62 J/mm^2 (SD = 0.05), much closer to the extrapolated cRDCB SERR, especially considering the uncertainty of actual cRDCB behavior at such large separations and the minor differences in fiber volume fraction (47% for cRDCB versus 53% for DCB specimens). It is also important to note that large-scale fiber bridging is inherently specimen-specific, so much so that different DCB specimen thicknesses produce different steady-state SERR values [2, 3, 30].

It is important to note that the cRDCB specimens were not loaded sufficiently to produce TSRs that completely captured unload behavior. This result is due to the small size of the cRDCB specimen in concert with the extensive degree of large-scale fiber bridging experienced by this E-glass/epoxy prepreg material, limiting the degree to which large-scale damage regimes could be assessed. Future testing to larger separations would allow the cRDCB specimen to assess more damage behavior, eliminating the uncertainty of extrapolated toughness values used in this paper. In addition, such work would help clarify how well the cRDCB captures fiber-bridging response compared to the DCB.

While the cRDCB specimen may exhibit less crack extension than the DCB specimens tested, there are many applications, such as low-velocity impacts [31–33] or fatigue damage initiation [5], where such extensive crack extension is not needed. Furthermore, the cRDCB has far greater sensitivity to and resolution of the early damage behaviors that dominate such applications. While the DCB specimen may provide better estimates of toughness at catastrophic levels of delamination, it is important to note that this measurement is a singular value and cannot be directly used in contemporary modeling techniques. The cRDCB, on the other hand, directly measures the TSR of Mode I delamination at all levels of crack extension, which can be inputted directly into CZM. It is only due to the specific combination of material system and specimen geometry used in this work that complete fibre bridging response was not captured.

Presently, the fabrication process of the cRDCB limits the materials that can be tested to prepreg tapes, whereas DCB specimens can be manufactured from a wide array of material classes and manufacturing techniques. While

prepreg tapes are commonly used for aerospace and other specialized components, other manufacturing methodologies are more frequently used in high-volume-production environments. However, future work will investigate adapting the cRDCB specimen to these other classes of materials. One option is to bond processed laminates to the metallic adherends using adhesive, similar to the work of Marzi et al. [17]. Although the adhesive would add compliance to the system, the use of DIC, as applied in the current study, will mitigate this issue. Compared to DCB, the cRDCB is more amenable to DIC analysis as the area in which damage occurs is relatively compact compared to the long, slender aspect ratio of the DCB specimen.

4 Conclusions

The composite rigid double cantilever beam (cRDCB) has demonstrated the ability to extract the complete traction-separation response (TSR) of Mode I delamination of an E-glass/epoxy laminate. While the cRDCB specimen exhibits less crack extension than contemporary methodologies, the specimen design has been shown to assess the onset of damage and early damage regimes with excellent sensitivity. With careful specimen preparation and fixturing, the cRDCB specimen exhibited variability comparable to traditional test methodologies.

The cRDCB results were in good agreement with the widely-accepted double cantilever beam (DCB) in terms of strain energy release rate (SERR) up to the onset of large-scale fiber bridging. Indeed, the cRDCB produced well-defined TSRs for this early damage behavior, which is not possible with the DCB. However, the results of the cRDCB and DCB deviate somewhat as fiber bridging began to dominate, which could be attributed to the small size of the cRDCB limiting crack extensions that could be attained. However, there are many applications where modeling of onset and initiation of delamination is of greater concern than catastrophic damage.

The ability to produce TSRs with excellent resolution in early damage behavior is beneficial for modeling applications where predicting the onset of damage is important, such as low-velocity impacts or low-cycle fatigue. While the cRDCB specimen is presently limited to prepreg laminates due to the processing methodology used herein, future work will adapt this test methodology to other classes of FRP laminate materials. Finally, the small

size and rigidity of the cRDCB specimen make it more suitable for high-deformation-rate testing than traditional, high-compliance specimens like the DCB, although such testing is beyond the scope of this work.

5 Acknowledgments

The authors would like to acknowledge the financial support of the Natural Science and Engineering Research Council of Canada (NSERC) and the Ontario Advanced Manufacturing Consortium (AMC).

6 Ethics Declarations

6.1 Conflicts of Interest

The authors declare no conflicts of interest.

Appendix A – Data Analysis Scheme for cRDCB Specimens

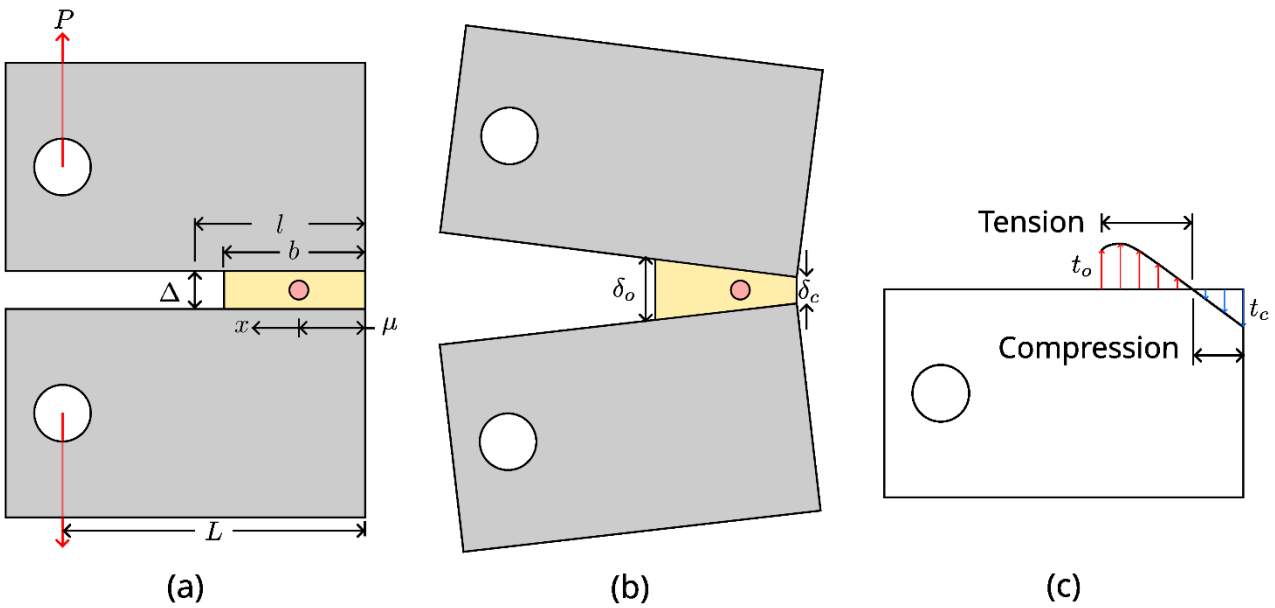

Fig. 11 Dimensions (a), deformed view (b), and free body diagram (c) of the cRDCB specimen used to derive the data processing method to extract traction-separation responses

This methodology is based heavily on the work of Watson et al. [19]. However, while Watson's methodology made use of displacement at the loading pin (dimension L in Fig. 11), the methodology was revised to use on-specimen

displacement at any point l on the specimen. In practice, l is often chosen to be as close to the crack tip (b) as possible.

The displacement at any point, x, along the delamination interface can be given by

$$\delta(x) = \frac{\Delta}{b-\mu}x \qquad (1)$$

Using this equation, we can relate displacement at the measured displacement, displacement at the crack tip, δ_o, and compressive displacement at the opposite the crack, δ_c.

$$\frac{\Delta}{l-\mu} = \frac{\delta_o}{b-\mu} = \frac{\delta_c}{\mu} \qquad (2)$$

If it is assumed that the compressive response of the delamination interface is linearly-elastic, peak compressive traction, σ_c, can be defined with respect to measured displacement and the stiffness of the material, K_I, where stiffness is defined as force divided by measured displacement, as shown later.

$$\sigma_c = \frac{K_I\mu}{l-\mu}\Delta \qquad (3)$$

Using the free-body diagram shown in Fig. 11, a force (equation (4) and moment (equation 5) balance can be computed assuming an arbitrary distribution of traction in tension

$$P + \frac{1}{2}\sigma_c\mu B = B\int_0^{b-\mu}\sigma(x)dx \qquad (4)$$

$$P(L-\mu) - \frac{1}{3}\mu^2\sigma_c B = B\int_0^{b-\mu}x\sigma(x)dx \qquad (5)$$

If we assume linear traction-separation behaviour in tension, one can relate peak tensile traction, σ_o, to peak compressive traction

$$\sigma_c = \frac{\mu\sigma_o}{b-\mu} = \frac{\mu K_i\Delta}{b-\mu} \qquad (6)$$

Using this relationship and subbing into equations (4) and (5), one can solve for initial stiffness K_I and the intial pivot location μ_e.

$$\mu_e = \frac{3Lb - 2b^2}{6L - 3b} \quad (7)$$

$$K_I = \frac{F}{\delta}\left(\frac{3(L-\mu_e)(l-\mu_e) - 2(l-\mu_e)(b-\mu_e)}{\mu_e^2 Bb}\right) \quad (8)$$

Substituting equation (8) into the force and moment balance equations (equations 4 and 5), as well as performing a change of variable for the integration to describe traction with respect to displacement, not position along the interface yields

$$P + \frac{\mu^2 K_I \Delta}{2(l-\mu)} = \frac{B(l-\mu)}{\Delta}\int_0^{\delta_o} \sigma(\delta)d\delta \quad (9)$$

$$P(L-\mu) - \frac{\mu^3 K_i \Delta}{3(l-\mu)} = B\left(\frac{l-\mu}{\Delta}\right)^2 \int_0^{\delta_o} \delta\sigma(\delta)d\delta \quad (10)$$

Differentiating these equations to isolate traction with respect to displacement (or separation) yields

$$\sigma(\delta) = \frac{d\Delta}{d\delta_o}\frac{d}{d\Delta}\left(\frac{P\Delta}{B(l-\mu)} + \frac{\mu^2 K_I \Delta^2}{2(l-\mu)^2}\right) \quad (11)$$

$$\sigma(\delta) = \frac{l-\mu}{\Delta(b-\mu)}\frac{d\Delta}{d\delta_o}\frac{d}{d\Delta}\left(\frac{P(L-\mu)\Delta^2}{B(l-\mu)^2} - \frac{\mu^3 K_I \Delta^3}{3(l-\mu)^3}\right) \quad (12)$$

There are two unknowns shared by these two equations: traction at the current separation, $\sigma(\delta)$, and the instantaneous pivot location, μ. Closed-form solutions for each are non-trivial, especially if one considers that μ is dependent on traction, which is dependent on measured force and displacement. To that end, an iterative root finding was adopted where instantaneous pivot location, μ, was solved for at every force and displacement provided, then used to compute traction.

It should be noted that Rajan et al. [21] presented a different processing scheme that also used on-specimen measurements. In particular, the Rajan method eliminated the iterative step of solving for pivot location by measuring both crack open (effectively l in this work) and compression opposite the delamination interface from the crack-tip. The methodology proposed by Rajan was investigated in this work but was difficult to implement since the precise compressive displacement of the specimen could not be measured due to edge effects in the DIC speckle pattern. Further, applying the method at a location away from the edge of the specimen did not improve the traction-separation outcome. Thus, the method by Watson was used in the current study.

References

[1] Tabiei A, Zhang W (2018) Composite Laminate Delamination Simulation and Experiment: A Review of Recent Development. Appl Mech Rev 70:. https://doi.org/10.1115/1.4040448

[2] Farmand-Ashtiani E, Cugnoni J, Botsis J (2015) Specimen thickness dependence of large scale fiber bridging in mode I interlaminar fracture of carbon epoxy composite. Int J Solids Struct 55:58–65. https://doi.org/10.1016/j.ijsolstr.2014.03.031

[3] Pappas GA, Botsis J (2020) Towards a geometry independent traction-separation and angle relation due to large scale bridging in DCB configuration. Compos Sci Technol 197:108172. https://doi.org/10.1016/j.compscitech.2020.108172

[4] Wisnom MR (2012) The role of delamination in failure of fibre-reinforced composites. Philos Trans R Soc Math Phys Eng Sci 370:1850–1870. https://doi.org/10.1098/rsta.2011.0441

[5] Yao L, Alderliesten RC, Benedictus R (2016) The effect of fibre bridging on the Paris relation for mode I fatigue delamination growth in composites. Compos Struct 140:125–135. https://doi.org/10.1016/j.compstruct.2015.12.027

[6] ASTM International (2013) ASTM D5528-13 Standard test method for mode I interlaminar fracture toughness of unidirectional fiber-reinforced polymer matrix composites. ASTM International, West Conshohocken, PA

[7] Compston P, Jar P-YB (1999) The Influence of Fibre Volume Fraction on the Mode I Interlaminar Fracture Toughness of a Glass-Fibre/Vinyl Ester Composite. Appl Compos Mater 6:353–368. https://doi.org/10.1023/A:1008973211347

[8] Frossard G, Cugnoni J, Gmür T, Botsis J (2016) Mode I interlaminar fracture of carbon epoxy laminates: Effects of ply thickness. Compos Part Appl Sci Manuf 91:1–8. https://doi.org/10.1016/j.compositesa.2016.09.009

[9] Lu X, Ridha M, Chen BY, et al (2019) On cohesive element parameters and delamination modelling. Eng Fract Mech 206:278–296. https://doi.org/10.1016/j.engfracmech.2018.12.009

[10] Gustafson PA, Waas AM (2009) The influence of adhesive constitutive parameters in cohesive zone finite element models of adhesively bonded joints. Int J Solids Struct 46:2201–2215. https://doi.org/10.1016/j.ijsolstr.2008.11.016

[11] Sørensen BF, Jacobsen TK (2009) Characterizing delamination of fibre composites by mixed mode cohesive laws. Compos Sci Technol 69:445–456. https://doi.org/10.1016/j.compscitech.2008.11.025

[12] Sørensen BF, Jacobsen TK (2003) Determination of cohesive laws by the J integral approach. Eng Fract Mech 70:1841–1858. https://doi.org/10.1016/S0013-7944(03)00127-9

[13] Gorman JM, Thouless MD (2019) The use of digital-image correlation to investigate the cohesive zone in a double-cantilever beam, with comparisons to numerical and analytical models. J Mech Phys Solids 123:315–331. https://doi.org/10.1016/j.jmps.2018.08.013

[14] Gunderson JD, Brueck JF, Paris AJ (2007) Alternative test method for interlaminar fracture toughness of composites. Int J Fract 143:273–276. https://doi.org/10.1007/s10704-007-9063-8

[15] Zhao Y, Seah LK, Chai GB (2016) Measurement of interlaminar fracture properties of composites using the J-integral method. J Reinf Plast Compos 35:1143–1154. https://doi.org/10.1177/0731684416642031

[16] Svensson D, Alfredsson KS, Biel A, Stigh U (2014) Measurement of cohesive laws for interlaminar failure of CFRP. Compos Sci Technol 100:53–62. https://doi.org/10.1016/j.compscitech.2014.05.031

[17] Marzi S, Rauh A, Hinterhölzl RM (2014) Fracture mechanical investigations and cohesive zone failure modelling on automotive composites. Compos Struct 111:324–331. https://doi.org/10.1016/j.compstruct.2014.01.016

[18] Dastjerdi AK, Tan E, Barthelat F (2013) Direct Measurement of the Cohesive Law of Adhesives Using a Rigid Double Cantilever Beam Technique. Exp Mech 53:1763–1772. https://doi.org/10.1007/s11340-013-9755-0

[19] Watson B, Liao C-H, Worswick MJ, Cronin DS (2018) Mode I traction-separation measured using rigid double cantilever beam applied to structural adhesive. J Adhes 1–21. https://doi.org/10.1080/00218464.2018.1502666

[20] ASTM International (2016) E647-15 - Standard Test Method for Measurement of Fatigue Crack Growth Rates. ASTM International, West Conshohocken, PA

[21] Rajan S, Sutton MA, McMakin W, et al (2020) Characterization of Mode I and Mode II traction–separation laws for cohesive separation of uncured thermoset tows. Int J Fract 221:25–38. https://doi.org/10.1007/s10704-019-00399-1

[22] ASTM International (2015) D3171-15 - Standard Test Methods for Constituent Content of Composite Materials. ASTM International, West Conshohocken, PA

[23] D'Errico J (2022) SLM - Shape Language Modeling. In: MATLAB Cent. File Exch. https://www.mathworks.com/matlabcentral/fileexchange/24443-slm-shape-language-modeling. Accessed 6 Sep 2022

[24] Brown D (2019) Tracker Video Analysis and Modeling Tool V5.1.3

[25] De Gracia J, Boyano A, Arrese A, Mujika F (2015) A new approach for determining the R-curve in DCB tests without optical measurements. Eng Fract Mech 135:274–285. https://doi.org/10.1016/j.engfracmech.2015.01.016

[26] Marat-Mendes R, Freitas MJ (2006) DCB , ENF and ECT Tests for Interlaminar Fracture of Glass/Epoxy Unidirectional Laminates. In: 10th Portuguese Conference on Fracture. University of Minho, Braga, Portugal, pp 1–7

[27] Marat-Mendes RM, Freitas MM (2010) Failure criteria for mixed mode delamination in glass fibre epoxy composites. Compos Struct 92:2292–2298. https://doi.org/10.1016/j.compstruct.2009.07.017

[28] Gilchrist MD, Svensson N (1995) A fractographic analysis of delamination within multidirectional carbon/epoxy laminates. Compos Sci Technol 55:195–207. https://doi.org/10.1016/0266-3538(95)00099-2

[29] Hashemi S, Kinloch AJ, Williams JM (1990) The analysis of interlaminar fracture in uniaxial fibre-polymer composites. Proc R Soc Lond Math Phys Sci 427:173–199. https://doi.org/10.1098/rspa.1990.0007

[30] Gong Y, Chen X, Li W, et al (2021) Delamination in carbon fiber epoxy DCB laminates with different stacking sequences: R-curve behavior and bridging traction-separation relation. Compos Struct 262:113605. https://doi.org/10.1016/J.COMPSTRUCT.2021.113605

[31] De Moura MFSF, Gonçalves JPM, Marques AT, De Castro PMST (1997) Modeling Compression Failure after Low Velocity Impact on Laminated Composites Using Interface Elements. J Compos Mater 31:1462–1479. https://doi.org/10.1177/002199839703101501

[32] Aymerich F, Dore F, Priolo P (2009) Simulation of multiple delaminations in impacted cross-ply laminates using a finite element model based on cohesive interface elements. Compos Sci Technol 69:1699–1709. https://doi.org/10.1016/J.COMPSCITECH.2008.10.025

[33] Zhang Y, Sun L, Li L, et al (2019) Experimental and numerical investigations on low-velocity impact response of high strength steel/composite hybrid plate. Int J Impact Eng 123:1–13. https://doi.org/10.1016/j.ijimpeng.2018.08.015